Electronic structure, magnetic properties and electrical resistivity of the $Fe_2V_{1-x}Ti_xAl$ Heusler alloys: experiment and calculation

2006 J. Phys.: Condens. Matter 18 10319

(http://iopscience.iop.org/0953-8984/18/46/002)

INSTITUTE OF PHYSICS PUBLISHING JOURNAL OF PHYSICS: CONDENSED MATTER

J. Phys.: Condens. Matter **18** (2006) 10319–10334 doi:10.1088/0953-8984/18/46/002

Electronic structure, magnetic properties and electrical resistivity of the $Fe_2V_{1-x}Ti_xAl$ Heusler alloys: experiment and calculation

A Ślebarski[1,3], J Goraus[1], J Deniszczyk[2] and Ł Skoczeń[1]

[1] Institute of Physics, University of Silesia, Uniwersytecka 4, 40-007 Katowice, Poland
[2] Institute of Materials Science, University of Silesia, 40-007 Katowice, Poland

E-mail: slebar@us.edu.pl

Received 6 July 2006, in final form 30 August 2006
Published 1 November 2006
Online at stacks.iop.org/JPhysCM/18/10319

Abstract

The aim of this work is to investigate electronic structure, magnetic properties and electrical resistivity of $Fe_2V_{1-x}Ti_xAl$ Heusler alloys. Numerical calculations give a pseudogap at the Fermi level for the majority-spin band of Fe_2TiAl and a magnetic moment larger than 0.9 μ_B, whereas the ground state of Fe_2VAl is calculated as a nonmagnetic semimetal with a very low total density of states at the Fermi level. In our calculations the remaining alloys of the $Fe_2V_{1-x}Ti_xAl$ series are nonmagnetic for $x < 0.1$ and weakly magnetic for $0.1 < x \leqslant 1$. The magnetic moment μ of the series of $Fe_2V_{1-x}Ti_xAl$ compounds scales with the number of valence electrons and fits well to the Slater–Pauling curve. We also present a study of the electronic transport properties and magnetic susceptibility. The resistivities $\rho(T)$ of Fe_2VAl and $Fe_2V_{0.9}Ti_{0.1}Al$ are large and exhibit a negative temperature coefficient $d\rho/dT$ of the resistivity between 2 and 300 K. Below 20 K, $\rho(T)$ also shows an activated character. The magnetic susceptibility of Fe_2VAl and $Fe_2V_{0.9}Ti_{0.1}Al$ shows a maximum at $\sim$2 K which could reflect either the disorder effect or the hybridization gap, characteristic of Kondo insulators.

1. Introduction

Metal–insulator (semiconductor) transitions are continuously studied in various correlated systems [1], for which the low-T dependences of the macroscopic physical properties, characteristic of the Landau theory of Fermi liquids [2], are observed with temperature $T \to 0$ for quantities such as the magnetic susceptibility χ, the linear specific-heat coefficient, $\gamma \equiv C/T$, and the electrical resistivity $\rho(T)$. Fe_2VAl has recently attracted a lot of attention in connection with possible d-electron heavy-fermion (HF) behaviour [3]. The resistivity of Fe_2VAl has a semiconducting-like behaviour, and the specific heat revealed an upturn in

[3] Author to whom any correspondence should be addressed.

$C(T)/T$ resembling that of conventional f-electron heavy-fermion compounds. Several band-structure calculations have been carried out, all of which found Fe_2VAl to be a nonmagnetic semimetal with a low carrier concentration and a small value of the density of states (DOS) at the Fermi level, ϵ_F, of $\sim$0.1 eV^{-1}. In this regard, Fe_2VAl shows an apparent similarity to a nonmagnetic narrow-gap semiconductor, FeSi, which has been classified as a unique d-electron Kondo insulator [4]. However, when the specific-heat measurements were carried out in high magnetic fields, they showed that the upturn in $C(T)/T$ was due to a Schottky anomaly arising from magnetic clusters, but not to Kondo interaction [5]. Also, the band structure calculations did not give evidence for HF behaviour in Fe_2VAl [6] and yield only a minor mass renormalization [7–10]; likewise, an infrared (IR) study did not show clear features of the HF state in the electrodynamic response of this compound [11]. It is a possible scenario that the antisite Fe defects, which induce localization of electrons in states close to the gap, produce the Schottky anomaly in the specific heat of Fe_2VAl and the negative giant magnetoresistance [6, 12], and do not support the HF feature, whereas bulk behaviour [13] (maximum in χ_{ac}) can be dominated by large clusters which exhibit superparamagnetism and the low-temperature freezing transition. Alternatively, Deniszczyk and Borgieł [14] have shown, using tight-binding linear muffin-tin orbital (TB-LMTO) numerical calculations, that the Fe antisite defects in the nonmagnetic Fe_2VAl give rise to the narrow, strongly correlated d-like band located just below the Fermi level. Taking into account the analysis of the one-particle electronic structure, they showed that the many-body investigations qualitatively follow the experimental observations. In view of the diverse opinions, we examined the solid solution $Fe_2V_{1-x}Ti_xAl$ to see the effect of the decreasing number of electrons (with increasing x) on the gap formation in Fe_2VAl, as well as to trace the changes in the ground state properties across the series.

We report electronic structure studies and magnetic properties of the $Fe_2V_{1-x}Ti_xAl$ system. In contrast to Fe_2VAl, the Fe_2TiAl compound has not heretofore been investigated in detail [15–17]. The aim of this work is to investigate the electronic structure, electrical resistivity and the ac magnetic susceptibility of $Fe_2V_{1-x}Ti_xAl$ to better characterize the system in terms of hybridized band gap or metallic behaviour depending on the system composition.

2. Experimental details

Polycrystalline samples of $Fe_2V_{1-x}Ti_xAl$ were prepared by arc melting the constituent elements on a water-cooled copper hearth in a high-purity argon atmosphere with an Al getter. Each sample was remelted several times to promote homogeneity and annealed at 800 °C for 10 days. The samples were examined by x-ray diffraction (XRD) and found to be single phase, of the $L2_1$-type structure. However, Fe_2TiAl in the ternary phase diagram was reported to exist as a two-phase mixture [18]. In recent work, Suzuki *et al* [16] presented the XRD pattern of Fe_2TiAl with a very small amount of the Fe_2Ti phase, which is magnetic below $\sim$200 K and could strongly complicate the magnetic susceptibility $\chi(T)$ of the Fe_2TiAl sample. Our XRD diffraction analysis revealed that after long annealing the Fe_2TiAl alloy consisted of a single phase. However, if Fe_2TiAl contains some amount of the Fe_2Ti phase, any effect of its magnetic character it should be observed in the susceptibility $\chi(T)$ data, which is discussed in section 4.

Electrical resistivity measurements were made using a standard four-wire ac technique. The magnetic susceptibility was measured in the 1.9–300 K regime by use of a commercial ac LakeShore susceptometer. The amplitude of the excitation field was 1 mT at a fixed frequency of 10 kHz.

The XPS spectra were obtained with monochromatized Al Kα radiation at room temperature using a PHI 5700 ESCA spectrometer. The polycrystalline sample was scraped

with a diamond file under a high vacuum of 6×10^{-10} Torr immediately before taking a spectrum. A very small amount of oxygen could barely be detected in the noise of the XPS spectra. The spectra were calibrated according to [19]. Binding energies were referenced to the Fermi level ($\epsilon_F = 0$).

3. Computational methods

The electronic structure of the ordered and stoichiometric Fe_2VAl and Fe_2TiAl compounds was calculated with different self-consistent *ab initio* methods. The introductory results were obtained with the use of the approximated tight-binding muffin-tin orbital (TB-LMTO) method [20], employing the atomic sphere approximation (ASA) [21] for the crystal potential. We carried out the calculations using the very accurate linear augmented plane wave (LAPW) method [22] and taking into account the general shape of the crystal potential (full potential) in order to estimate the effect of the ASA. To account for the spin–orbit (SO) interaction exactly within a set of valence states we performed the fully relativistic calculations employing the full potential local orbital (FPLO) method [23].

Within the all-electron TB-LMTO approach the core states were treated in the full relativistic manner, while the valence states were calculated with the use of a scalar relativistic approximation which neglects the spin–orbit interaction. The LSDA exchange–correlation (XC) potential was taken in the form described by von Barth and Hedin [24], and the Langreth, Mehl and Hu (LMH) [25] generalized gradient (GG) corrections for the nonlocal character of the XC potential were taken into account. In the approximate TB-LMTO method the crystal potential is treated within the ASA approximation with overlapping Wigner–Seitz (WS) spheres centered at atomic positions, where the radii of the WS spheres are the parameters of the ASA-based methods. The values of the WS sphere radii were determined in such a way that the sum of all atomic sphere volumes is equal to the volume of the unit cell. We note, however, that the choice of the WS radii is of minor importance, which results from our previous calculations of the charge and spin density distributions within the unit cell of iron aluminides [26]. In the TB-LMTO calculations we assumed the volumes of WS spheres to be equal for all constituent atoms. To correct the effect of overlapping WS spheres we also included the combined-correction terms [27]. Basis functions up to $l = 2$ were included for all constituent atoms explicitly, and the $l = 3$ functions were included via the downfolding procedure [28]. The calculations were performed for 2769 $\vec{k}$-points in the irreducible wedge of Brillouin zone (BZ), with the total energy error less then 0.01 mRyd. Further increase of $\vec{k}$-points did not change the total energy in the significant way. The calculations were performed with the use of TB LMTO-4.7 code [29].

In the FP-LAPW approach no shape approximation is used and the crystal potential is expanded into spherical (lattice) harmonics within the muffin-tin (MT) atomic spheres and into plane waves outside MT spheres. MT spheres of radii 2.3 and 2.2 au were assumed for transition metal (Fe, V, Ti) and Al atoms, respectively. The fully relativistic and scalar-relativistic formalism was applied for the core and valence states, respectively. The spin–orbit interaction for the valence states was included applying the second variational method [22]. The XC potential within the LSDA + GG approximation scheme was employed in the form developed by Perdew *et al* [30]. The valence basis set including the 4s4p3d atomic orbitals for transition atoms and 3s3p for aluminium was assumed. To correct for the linearization errors the following set of the local orbitals [31] was assumed: {3s, 3p} for transition metal atoms and {2s, 2p} for aluminium atom. In the tetrahedron integrations 816 $\vec{k}$-points in the irreducible wedge of the BZ were used. The $\vec{k}$-vectors together with a $R_{mt} \times K_{\max}$ parameter of 9.0 resulted in a total energy error smaller than 0.1 mRyd. The calculations were performed using the WIEN2K code [32].

The fully relativistic FPLO calculations were performed using the LSDA XC potential of Perdew and Wang [33]. The basis set of 4s4p3d local orbitals for transition metal (TM) atoms and 3s3p3d local orbitals for aluminium atom were assumed. The 3s3p states of TM atoms and 2s2p states of Al were separated to a group of orbitals of semicore type. The spatial extension of the valence orbitals of the FPLO method is controlled by the confining power-law potential. In the calculations a confining potential exponent equal to 4.0 was chosen. For the ordered end-point compounds in the $\vec{k}$-space integration a mesh of 349 $\vec{k}$-points in the irreducible wedge of the BZ was chosen. The assumed calculation setup gave a $\vec{k}$-space total energy convergence within an error less than 10^{-4} Ryd. Changes in the electronic and magnetic structure of $Fe_2V_{1-x}Ti_xAl$ alloys were investigated by means of the extended FPLO method [34] employing the Blackman *et al* [35] matrix generalization of the coherent potential approximation (CPA) to describe the atomic disorder in bulk materials. The calculation setup used was the same as that in the FPLO calculations of ordered compounds. The calculations were performed for the Ti concentrations $x = 0.1$, 0.125, 0.25, 0.4, 0.6, 0.7, 0.875 and 0.9. The investigations using the FPLO and FPLO-CPA methods were performed using the FPLO-5 release of the fully relativistic code of FPLO method [36].

To test the possible formation of the magnetic clusters due to the short-range order effect we investigated the electronic and magnetic structure of two off-stoichiometric compositions of $Fe_2V_{1-x}Ti_xAl$ alloy with $x = 0.125$ and $x = 0.875$ using the *supercell* approach. With this aim we have used the *supercell* with translation vectors (0, 2a, 2a), (2a, 0, 2a) and (2a, 2a, 0) of the underlying $L2_1$ cubic lattice, i.e., including 32 atoms. The superstructures with $x = 0.125$ and $x = 0.875$ were constructed by replacing one V atom by Ti in the $8 \times (Fe_2VAl)$ *supercell* and one Ti atom by V in the $8 \times (Fe_2TiAl)$ *supercell*, respectively. The supercell approach allows for distinguishing formally equivalent atomic sites which due to atomic defects and different local atomic coordination become chemically (crystallographically) inequivalent. The calculations for the superstructures were performed with the use of the TB-LMTO method assuming the same calculation setup as that described for the ordered stoichiometric materials. Due to the large dimensions of the supercells used in calculations the total energy versus the number of $\vec{k}$-vectors convergence error less than 0.1 mRyd was achieved by assuming a $\vec{k}$-mesh of only 72 points in the irreducible wedge of the BZ. To gain better statistics in the density of states calculations using the tetrahedron method an additional iteration with 413 $\vec{k}$-vectors in the irreducible wedge of the BZ was performed.

4. Results and discussion

4.1. Electronic structure: experiment and calculations

X-ray photoemission spectroscopy is a powerful technique for studying the electronic properties of solids near the Fermi level. Such studies are used to determine the total densities of states of the alloy. However, the contribution of the constituent elements to the valence bands (VBs) is possible to be obtained, when the VB XPS spectra are closely compared with the calculated ones. In this section we compare the experimental VB XPS spectra and the VB calculations for Fe_2VAl and Fe_2TiAl.

In figure 1 we show the calculated total and partial atomic DOSs obtained for Fe_2VAl by different methods. Also shown in the figure, for comparison, are the XPS VB spectra corrected for the background and the calculated XPS spectra curves, for which the LMTO and LAPW partial densities of states were convoluted by a Lorentzian with a 0.4 eV half-width to account for the instrumental resolution and multiplied by the corresponding cross sections for partial states of Fe, V, and Al with different l-symmetry, taken from [37]. The

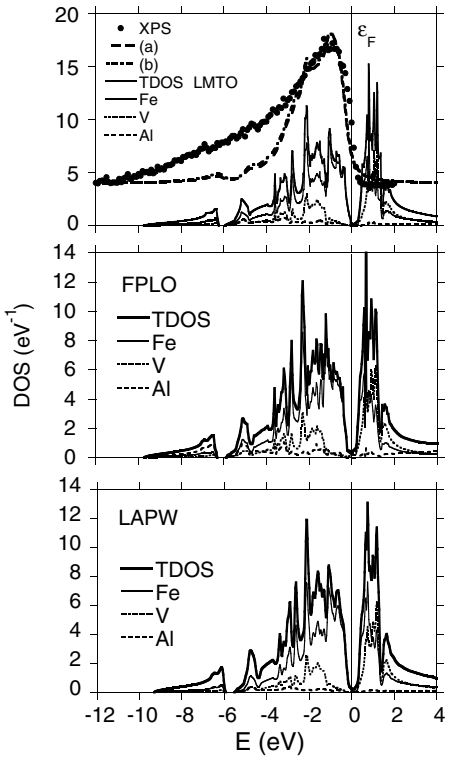

Figure 1. The total density of states (DOS) calculated for Fe_2VAl with the use of different approaches: spin-polarized TB LMTO, spin-polarized FPLO, and spin-polarized LAPW. The partial densities of states of Fe, V and Al are also shown. The LMTO (curve a) and LAPW with SO interaction (curve b) DOSs, convoluted with Lorentzian of half width 0.4 eV, taking into account proper cross sections for bands with different l symmetry (curve with larger thickness), compared to the measured VB XPS data (points) obtained for Fe_2VAl, corrected for background, are also plotted (intensities in arbitrary units). The SO interaction is of minor importance for the shape of the calculated XPS spectra. Note that the zero of the energy scale is shifted to the Fermi level.

energy spectra of the electrons were analysed with an energy resolution better than 0.4 eV. In general, there is a qualitative agreement between the XPS spectra obtained experimentally and the calculated ones. However, in the near vicinity of the Fermi level, and between ∼3 and 10 eV below ϵ_F, the agreement is not so good, which we explain as follows. In Heusler-type alloys the electronic structure strongly depends on the local ordering. The calculated spectra which are presented in figure 1 (also in figure 2) have been obtained for the stoichiometric and ordered compounds. It is well documented [14, 38] that in disordered Fe_2VAl the Fe and V atoms at the antisite positions (Fe $\leftrightarrow$ V) give rise to a narrow impurity d band located just in the middle of the quasi-gap calculated for an ordered Fe_2VAl compound. This narrow d band formed by the antisite Fe atoms in the Fe_2VAl alloy can significantly change the shape of the XPS spectra measured with an energy resolution of ∼0.4 eV near the Fermi level, whereas the calculated XPS DOSs in figure 1 do not include this effect. Note that the high-resolution XPS valence bands clearly show a feature attributed to an antisite Fe contribution [39].

At higher binding energies the physical origin of the discrepancy between the calculated and measured XPS spectra is not clear. It can also be attributed to the atomic disorder. Another

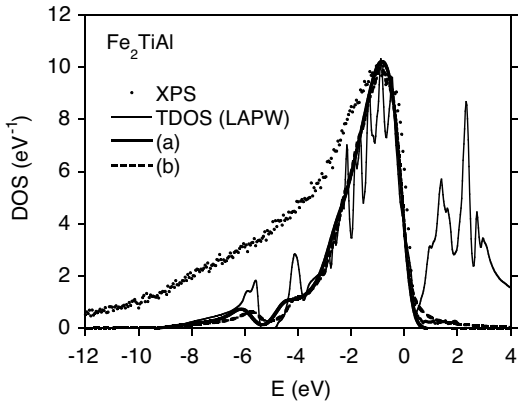

Figure 2. The total DOS calculated for Fe_2TiAl with the use of spin polarized LAPW. The LAPW LSDA + GGA DOSs (curve a) and LAPW LSDA + GGA + SO DOSs (curve b), convoluted with a Lorentzian of half-width 0.4 eV, taking into account proper cross sections for bands with different *l*-symmetry, compared to the measured VB XPS data (points) obtained for Fe_2TiAl, corrected for background, are also plotted (intensities in arbitrary units). Curve b shows a negligible divergence in its shape near the Fermi level, when we turn off the SO interaction in the LAPW calculations. Note that the zero of the energy scale is shifted to the Fermi level.

reason could be a modelling character of background subtraction. In figures 1 and 2 the XPS spectra obtained experimentally are reduced by subtracting the backgrounds which have been calculated with approximate (although well validated) Tougaard algorithms [40].

In figure 1 the total DOS spectrum decomposes into two clearly separated parts. A band located in the binding energy range of 6–9 eV originating mainly from the s states of Al is separated by a gap of ∼0.3 eV from the valence band. The p states of Al hybridize with the d states of Fe and V atoms to form a band visible in the binding energy range 3–5.5 eV. The upper part of the valence band, where the maximum in the DOS occurs, is mainly composed of Fe d states. The shape of the DOS generally does not depend on the method used for calculations, excluding the energy range of ∼1 eV in the vicinity of ϵ_F (see table 1). Fe_2VAl appears semimetallic in LMTO and LAPW calculations with the DOS at the Fermi level of ∼0.3 eV^{-1}. In LAPW band structure calculations we observed a very similar effect to that reported in [8], namely, the spin–orbit coupling reduces the DOS at ϵ_F from 0.37 to ∼0.25 eV^{-1}. The fully relativistic FPLO method, which treats exactly the spin–orbit interaction within the set valence states, also gives a reduced value of DOS at ϵ_F, as compared to that calculated within a semi-relativistic formalism.

Shown in figure 2 is a comparison of the total DOS of Fe_2TiAl calculated by the spin-polarized LAPW method and both measured and calculated XPS VB spectra. The LAPW calculations predicted a pseudogap in the total DOS located 0.45 eV above the Fermi level with the value of ∼0.6 eV^{-1}. The bands located between ∼5 and 9 eV originate mainly from the s states of Al, and as in Fe_2VAl the d states are located near the Fermi level. The XPS curves of the magnetic Fe_2TiAl calculated within the LAPW or LMTO method are compared favourably with the experimental data. The discrepancy between the experimental and calculated XPS spectra discussed above, is again visible at higher binding energies and in the near vicinity of the Fermi level.

In figure 3 we present numerical calculations of the electronic density of states of Fe_2TiAl. All the methods, LMTO, FP-LAPW and FPLO, give a small DOS of ∼0.20 eV^{-1} at ϵ_F for the majority-spin band, whereas the minority-spin band is metallic, which leads to a non-integer

Table 1. Heusler alloys investigated and their structural and calculated magnetic properties: the spin-polarized (↑ or ↓) DOS at ϵ_F and the magnetic moment μ.

		DOS at ϵ_F (eV^{-1})				
Compound	a (Å)	↑	↓	Nonmagnetic	Method	μ (μ_B)
Fe_2VAl	5.766			0.28	LMTO	0
				0.37	LAPW LSDA	0
				0.25	LAPW LSDA + SO	0
				0.14	FPLO	0
$Fe_2V_{0.9}Ti_{0.1}Al$	5.773	—	—	—	FPLO CPA	0
$Fe_2V_{0.875}Ti_{0.125}Al$				0.78	LMTO	0
		—	—	—	FPLO CPA	0.03
$Fe_2V_{0.7}Ti_{0.3}Al$	5.795	—	—	—	FPLO CPA	0.123
$Fe_2V_{0.6}Ti_{0.4}Al$	5.806	—	—	—	FPLO CPA	0.255
$Fe_2V_{0.4}Ti_{0.6}Al$	5.822	—	—	—	FPLO CPA	0.498
$Fe_2V_{0.3}Ti_{0.7}Al$	5.838	—	—	—	FPLO CPA	0.611
$Fe_2V_{0.125}Ti_{0.875}Al$		0.16	3.54		LMTO	0.825
		—	—	—	FPLO CPA	0.794
$Fe_2V_{0.1}Ti_{0.9}Al$	5.863	—	—	—	FPLO CPA	0.806
Fe_2TiAl	5.892	0.15	3.63		LMTO	0.952
		0.20	3.65		LAPW LSDA	0.945
		0.25	3.76		LAPW LSDA + SO	0.935
		0.22	3.60		FPLO	0.938

spin moment of ∼0.94 μ_B (see table 1). We also noted that the spin–orbit effect slightly enhances the value of the DOS at the Fermi level from 0.2 to 0.25 eV^{-1} for the majority-spin band and from 3.65 to 3.76 eV^{-1} for the minority-spin band; it also slightly reduces the magnetic moment of Fe_2TiAl from 0.945 to 0.935 μ_B.

Figure 4 shows the LMTO DOSs calculated for the $Fe_2V_{0.875}Ti_{0.125}Al$ and $Fe_2V_{0.125}Ti_{0.875}Al$. The sample with $x = 0.125$ of the $Fe_2V_{1-x}Ti_xAl$ series displays pseudometallic and nonmagnetic character, whereas the sample with $x = 0.875$ is an almost half-ferromagnetic metal. For both compositions our *supercell* calculations give no evidence for the formation of magnetic clusters due to V ↔ Ti off-stoichiometry.

Figures 5 and 6(b) exhibit in detail the electronic bands and the DOSs of the members of the $Fe_2V_{1-x}Ti_xAl$ series in the vicinity of the Fermi level. Figure 5 clearly shows that the spin-polarized band structure of Fe_2TiAl can be related to that of paramagnetic Fe_2VAl split due to exchange interaction. The shift of the spin-polarized bands is not symmetric and some detailed differences between band structures of both compounds are observed. Namely, in Fe_2VAl the parabolic band of d_{eg} states of vanadium, which gives the electronic pocket at the X-point in the BZ, is not present in the vicinity of ϵ_F for Fe_2TiAl. The corresponding states of the Ti atom are less bounded and shifted to higher energies without any contribution to the DOS at the Fermi level. Likewise, the d-t_{2g} states of Fe in Fe_2VAl form a parabolic band at the Γ-point which has hole character, and then form a narrow band located just below ϵ_F, whereas in Fe_2TiAl the Fe d-t_{2g} majority-spin bands are shifted above ϵ_F. At the Γ-point of the BZ of Fe_2TiAl the gap characteristic for the Fe_2VAl compound disappears in the majority-spin band structure, whereas the minority-spin band structure of Fe_2TiAl is simply the replica of that of paramagnetic Fe_2VAl; however, the bands are shifted to higher energies ∼0.7 eV. As a consequence, the band structure of the magnetic Fe_2TiAl compound is of metallic character. Figure 6(b) shows the evolution of the LMTO DOS in the surroundings of ϵ_F in the series of

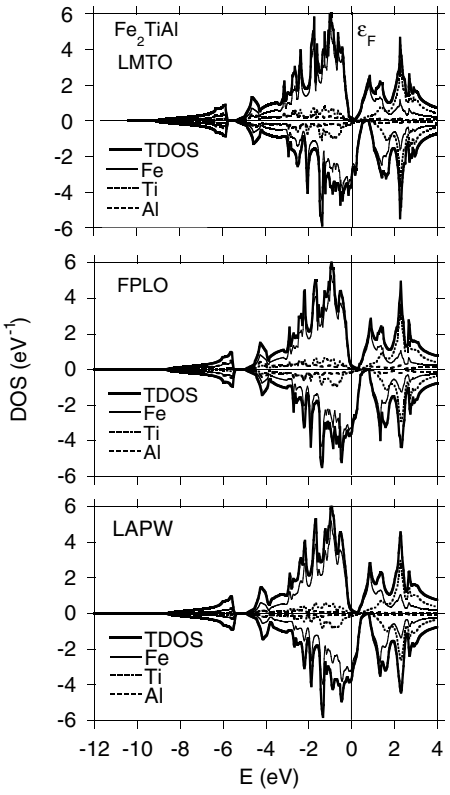

Figure 3. The spin-polarized total DOS calculated for Fe_2TiAl with the use of three different approaches: TB LMTO, FPLO, and LAPW LSDA + GGA, respectively. The partial densities of states of Fe, Ti, and Al are also shown. The top panels exhibit the majority-spin DOS. Note that the zero of the energy scale is shifted to the Fermi level.

the $Fe_2V_{1-x}Ti_xAl$ alloys versus concentration of Ti. The change in DOS versus x observed in the figure suggests the following explanation for the onset of magnetism in the series of $Fe_2V_{1-x}Ti_xAl$ alloys. The increasing content of Ti changes the number of d-type electrons. For the members of the $Fe_2V_{1-x}Ti_xAl$ series rich in V ($x \leqslant 0.1$), the small decrease of the number of 3d electrons (<10%) causes a distinct shift of the Fermi level towards the top of the valence band. In consequence, the DOS at ϵ_F increases gradually; however, this is not enough to fulfil the Stoner criterion for magnetic order. The DOSs at ϵ_F satisfy the Stoner criterion for $x > 0.1$ (see figure 6) and the members of the $Fe_2V_{1-x}Ti_xAl$ system with the concentration of Ti larger than ∼10% become magnetic. The majority-spin bands shift towards higher binding energy, giving a pseudogap at the Fermi level. The minority-spin bands shift continuously toward higher energies too, and as a result give the half-metallic character of the bands at ϵ_F. Figure 6(a) and table 1 summarize the magnetic properties calculated for the investigated alloys. Figure 6(a) displays the magnetic behaviour of the $Fe_2V_{1-x}Ti_xAl$ alloys resulting both from FPLO-CPA and TB-LMTO supercell calculations, which also proves that the magnetic polarization of V and Ti atoms is in opposite direction to the Fe local moment which is dominant, and determines the direction and magnitude of the total magnetic moment.

In table 1 the DOSs at ϵ_F are listed along with the calculated magnetic moments μ. In the series, the shape of the DOS is strongly dependent on doping (on x). The pseudogap of Fe_2VAl in the LMTO and LAPW approach disappears in the scalar-relativistic FPLO-CPA calculations, when V is replaced by more than 10% of Ti.

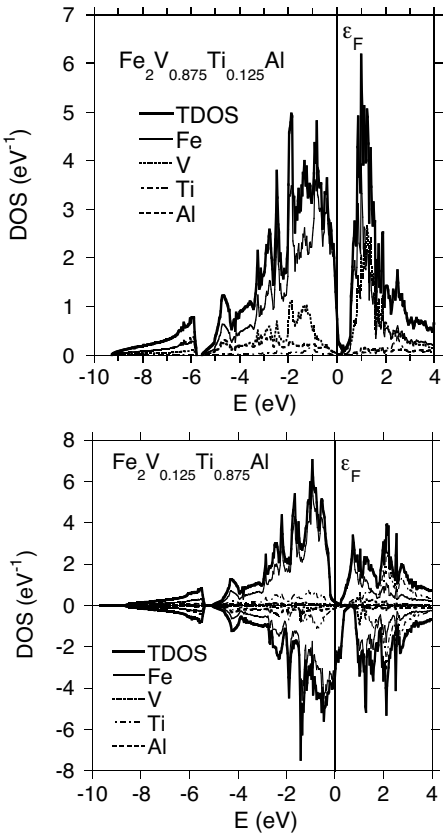

Figure 4. The total DOS calculated by TB-LMTO *supercell* approach for the $Fe_2V_{0.875}Ti_{0.125}Al$ and $Fe_2V_{0.125}Ti_{0.875}Al$ alloys; the partial DOSs are also presented. The top panels display the majority-spin DOS. Note that the zero of the energy scale is shifted to the Fermi level.

4.2. Electrical resistivity and magnetic susceptibility

In figure 7 we display the temperature dependence of the electrical resistivity $\rho(T)$ normalized to the $\rho(T = 300\ \mathrm{K})$ for various $Fe_2V_{1-x}Ti_xAl$ samples. The resistivities of the Ti-rich samples (i.e., for $x \geqslant 0.3$) are metallic and very similar in behaviour. The curves in figure 7 exhibit a typical behaviour of metals with an atomic disorder, with a residual resistivity of $\sim 1\ \mu\Omega$ m. In this plot one can distinguish Fe_2VAl and $Fe_2V_{0.9}Ti_{0.1}Al$; the resistivities of both samples are highly unusual, as they remain—for metallic systems—large (~ 27 and $\sim 15\ \mu\Omega$ m, respectively) and exhibit a negative temperature coefficient of the resistivity (TCR), $\mathrm{d}\rho/\mathrm{d}T < 0$, down to the lowest temperatures. The origin of the negative TCR effect is usually attributed to the strong atomic disorder. Mooij [41] studied the transport properties of a number of transition-metal alloys, finding that high resistivity and negative TCR are a *universal* property of many. However, the remaining $Fe_2V_{1-x}Ti_xAl$ alloys with $x > 0.1$ in figure 7 do not display a negative TCR, though they are disordered too. We therefore conclude that the negative TCR also results from the semimetallicity of both Fe_2VAl and $Fe_2V_{0.9}Ti_{0.1}Al$ samples. The resistivities of these alloys obey the relationship $\rho(T) = a + bT + \mathrm{e}^{\Delta E/T}$, with the parameters listed in table 2. $\Delta E \neq 0$ means that the insulating state is formed at low temperatures with a narrow gap ($2\Delta E \cong 3$ K) in the electronic density of states. This result seems to reflect the band structure calculations, which predicted the V-shape pseudogap at the Fermi level either for the ordered Fe_2VAl compound or disordered alloy. The V-shape pseudogap in the DOSs at the Fermi level could be a reason for either the high

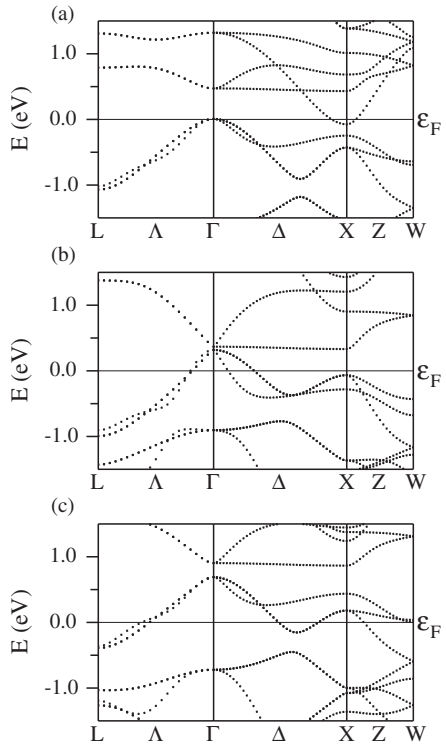

Figure 5. Band structure calculated with the use of the FP-LAPW method along selected high-symmetry lines in the vicinity of the Fermi level. (a) shows the bands of paramagnetic Fe_2VAl, (b) and (c) present respectively the majority-spin and minority-spin bands of ferromagnetic Fe_2TiAl. Note that the zero of the energy scale is shifted to the Fermi level.

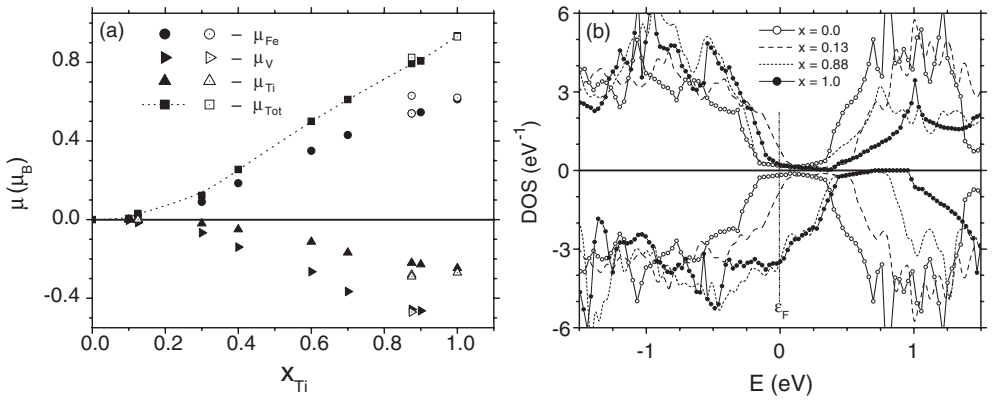

Figure 6. (a) The local atomic and total magnetic moments versus Ti concentration in the series of $Fe_2V_{1-x}Ti_xAl$ alloys. Solid symbols show the results of FPLO-CPA calculations, and open symbols give the results of calculations using the TB-LMTO method. (b) The DOS calculated with the use of the TB-LMTO method in the vicinity of the Fermi level. In the TB-LMTO calculations for non-stoichiometric compositions the *supercell* methodology was utilized. Note that the zero of the energy scale is shifted to the Fermi level.

resistivity or the small value of ΔE. Very similar $\rho(T)$ data were previously presented by Feng *et al* in [6].

Shown in figures 8(a)–(c) are magnetic susceptibility χ_{ac} data plotted as χ versus T and χ^{-1} versus T between 2 and 300 K for $Fe_2V_{1-x}Ti_xAl$. The susceptibilities for Fe_2VAl and

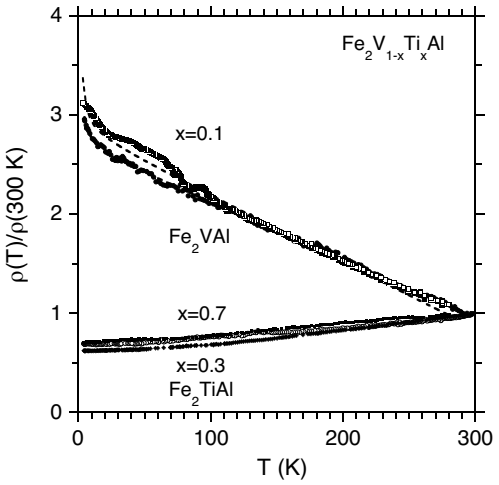

Figure 7. Reduced electrical resistivity $\rho(T)/\rho(300\ \mathrm{K})$ versus T for $Fe_2V_{1-x}Ti_xAl$. The $\rho(T)$ data for Fe_2VAl and $Fe_2V_{0.9}Ti_{0.1}Al$ are well described by a function $\rho(T) = a + bT + e^{\Delta E/T}$ (dotted curve). The remaining ρ-curves are plotted for the samples $x = 0.7$, 0.3, and 0.

Table 2. $Fe_2V_{1-x}Ti_xAl$: resistivity ρ obtained at $T = 300$ K, and a, b, and ΔE parameters for the best fits of the equation $\rho(T)/\rho(300\ \mathrm{K}) = a + bT + e^{\Delta E/T}$ to the experimental data (see figure 5).

$Fe_2V_{1-x}Ti_xAl$ x	ρ at 300 K ($\mu\Omega$ m)	a	b (K^{-1})	ΔE (K)
0	27.5	1.68	-5.77×10^{-3}	1.3
0.1	15.3	1.87	-6.84×10^{-3}	1.7
0.3	2.6		Metallic	
0.5	1.2		Metallic	
0.7	2.4		Metallic	
0.9	1.5		Metallic	
1	1.4		Metallic	

Table 3. The ac susceptibility parameterizations of the $Fe_2V_{1-x}Ti_xAl$ samples; $\chi_1 = \chi_0 + C/(T - \theta)$ follows a modified Curie–Weiss law and $\chi_2 = C/(T - \theta)$ expresses the Curie–Weiss law. The effective magnetic moment $\mu_{\mathrm{eff}} = \mu_B^{-1}(3k_BC/N_A)^{1/2}$.

		χ_1			χ_2	
$Fe_2V_{1-x}Ti_xAl$ x	ΔT-range (K)	χ_0 ($m^3\ mol^{-1}$)	θ (K)	μ_{eff} (μ_B)	μ_{eff} (μ_B)	θ (K)
0	2–14	46.5×10^{-10}	1.5	0.14		
0.1	6–80	56.5×10^{-10}	4.8	0.24		
0.3	60–300				3.48	−72.5
0.5	60–300				3.67	−56
0.7	60–300				3.62	−50.6
0.9	60–300				3.24	−58.5
1	97–300	20.1×10^{-10}	89.5	0.50		

$Fe_2V_{0.9}Ti_{0.1}Al$ shown in figure 6(a) cannot be explained by the Curie–Weiss (CW) law, but the data show that $\chi(T)$ obeys the *modified* CW law in the limited temperature range. The fit parameters to the equation $\chi(T) = \chi_0 + C/(T - \theta)$ are listed in table 3. The small θ value suggests weak magnetic behaviour at low temperatures.

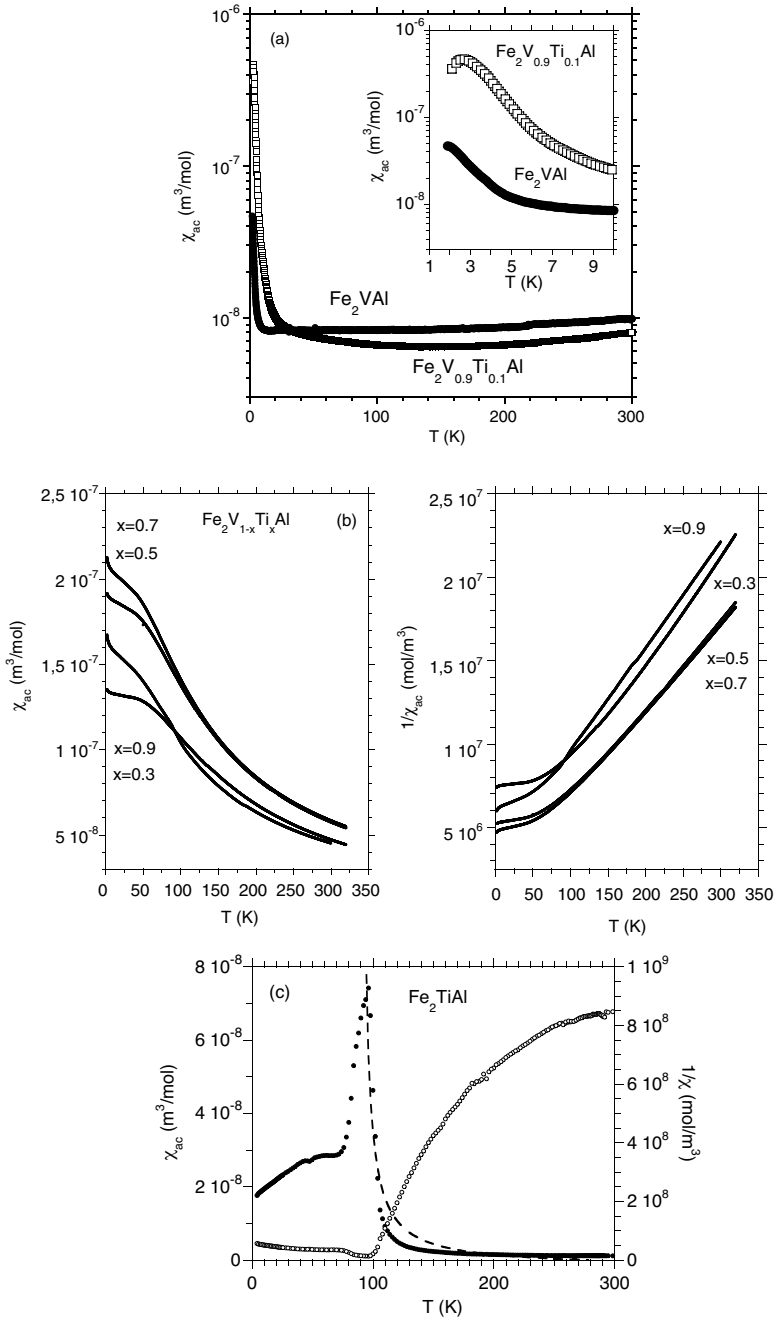

Figure 8. Temperature dependence of the ac susceptibility for Fe_2VAl and $Fe_2V_{0.9}Ti_{0.1}Al$ (a). The inset shows χ_{ac} versus T below 10 K. (b) The ac susceptibility χ and χ^{-1} versus T for $Fe_2V_{1-x}Ti_xAl$ system, where $x = 0.3$, 0.5, 0.9, and 0.7, respectively. (c) Temperature dependence of the ac susceptibility χ and χ^{-1} and the fit of the modified CW law (dotted line).

A prominent maximum in χ is observed for $Fe_2V_{0.9}Ti_{0.1}Al$ at $\sim$2.7 K, while for Fe_2VAl susceptibility markedly indicates a similar behaviour; however, this is at a lower

temperature than $T = 2$ K. A similar maximum previously reported for Fe_2VAl [13], and investigated versus excitation frequencies at different magnetic fields, was discussed as a result of superparamagnetic behaviour. The main conclusion of this work is that the stoichiometric Fe_2VAl is nonmagnetic; however, it contains antisite Fe defects which exhibit local magnetic moments, and also ferromagnetic regions which lead to the superparamagnetic behaviour. As continuation of this work, Feng *et al* [6] argued that the antisite disorder causes significant modification of the semimetallic band structure proposed theoretically, and leads to the localization of the d states, which form a large DOS near ϵ_F, whereas away from ϵ_F there are delocalized electrons which could give a negative TCR.

Our investigations of Fe_2VAl display that the measured values of χ at the lowest temperatures are one order of magnitude smaller than that previously obtained in [13]; also, the maximum in χ is shifted to a lower temperature. We attribute both these effects to the quality of our sample, which has a lower concentration of antisite defects. The maximum χ-value of the $Fe_2V_{0.9}Ti_{0.1}Al$ sample increases, which has more antisite defects due to alloying. However, the χ_{ac} maximum is not visible in the susceptibility $\chi(T)$ data for the remaining members of the series. Therefore, we speculate that the hybridized gap could also be an essential contribution to the abnormal low-T behaviour in $\chi(T)$; this will be discussed latter.

In figure 8(b) we show the magnetic susceptibility χ for $Fe_2V_{1-x}Ti_xAl$, where $0.3 \leqslant x \leqslant 0.9$ deviates markedly from the $\chi(T)$ data displayed in figure 8(a). All the $\chi(T)$ curves between 60 and 300 K can be described well by the CW law with very similar fit parameters, listed in table 3. The characteristic temperatures $\theta = \sim -60$ K for all samples indicate an antiferromagnetic ground state with predominantly antiferromagnetically coupled Fe magnetic moments. The constants C have a value that is close to the value of C expected for an iron configuration d^7Fe^{3+}, if one assumes that the angular momentum of the Fe ions is quenched in the disordered alloy, i.e., $J = S$ and $g_J = 2$.

In figure 8(c) we display the ac susceptibility versus temperature for Fe_2TiAl. The $\chi(T)$ data exhibit a different temperature dependence characteristic for the samples $0.3 \leqslant x \leqslant 0.9$ displayed in figure 6(b); it shows at 96 K a knee-shaped phase transition, which is very similar to the case in PdFeMn [42] or $LaFe_7Al_6$ [43], indicative of a transition to an inhomogeneous ferromagnet (*mictomagnet*). The inhomogeneous ferromagnetic state may be understood as a mutually blocked assembly of magnetic clusters. The effect cannot be attributed to the presence of the second phase Fe_2Ti, which is antiferromagnetically ordered at ~200 K [44, 45]. The susceptibility is well fitted by the modified CW law above T_C (see table 3).

4.3. Discussion

In [11] it has been shown from the optical conductivity data that Fe_2VAl has a deep pseudogap of ~0.1 eV at ϵ_F, which is highly unusual for intermetallic compounds. It also has been speculated that the resistivity of Fe_2VAl reflects a mixture of an electron excitation process over a pseudogap in the high-temperature range, and spin-dependent scattering from impurities at low T. Independently, crystallographic disorder resulting from atomic site exchange between Fe and V atoms can lead to the formation of ferromagnetic clusters which could give a reason for the ac susceptibility maximum, and explain the origin of the negative TCR effect. So far, however, a detailed understanding of the ground state properties of Fe_2VAl is lacking. The conclusion that the physical properties of the nonmagnetic Fe_2VAl are dominated by crystallographic disorder is generally accepted, while Kondo insulating behaviour seems not to play an important role. Alternatively, there are also some reports [14] that the Fe antisite defects give rise to the narrow, strongly correlated d-like band located almost at ϵ_F. In view of contradictory versions of the physical properties of Fe_2VAl, we concentrate below on the ac magnetic susceptibility, which has maximum first before reaching the $\chi \rightarrow 0$ limit on

further decreasing T. The maximum in χ is reached at $T < 2$ and ∼2.7 K for Fe_2VAl and $Fe_2V_{0.9}Ti_{0.1}Al$, respectively, and agrees well with the value of the gap Δ obtained from the fits to the resistivity. This maximum is not observed in the susceptibility of the remaining $Fe_2V_{1-x}Ti_xAl$ samples ($x > 0.1$) which contain antisite Fe defects too, and are (weakly) magnetic. If the χ-maximum were purely of spin-glass nature, it also should be observed in $\chi(T)$ data obtained for the $x > 0.1$ members of the series; this is, however, not the case. Our measurements suggest that the gap in Fe_2VAl is rapidly suppressed even by a small amount of Ti, suggesting the importance of changing (decreasing) the number of the conduction electrons, concomitant with increasing the x value, on the gap formation. A similar effect of the decreasing number of conduction electrons on the Kondo gap in CeRhSb, when Sb is substituted by Sn, was very recently discussed in [46]. At the critical concentration $x_c = 0.12$ the singlet Kondo state in $CeRhSb_{1-x}Sn_x$ characterized by $\chi(T \to 0) \to 0$ for $x \leqslant x_c$ is destroyed and the magnetic state appears. Similar features of the low-temperature $\chi(T)$ and $\rho(T)$ in CeRhSb and Fe_2VAl would suggest the Kondo lattice insulating gap of Fe_2VAl in nature which, however, should be modified by the atomic disorder. A paramagnetic Kondo insulator discussed within a periodic Anderson model provides an insulating state for a **k**-independent hybridization and for an even number of electrons per unit cell [47]. The stability of the paramagnetic versus magnetic ground state in the Kondo lattice limit is strongly dependent on the number of electrons per atom; therefore the energy gap should be very sensitive to the partial heteroelectronic substitution [48–50]. This is the case of Fe_2VAl, having 24 electrons/cell, when V is in part replaced by Ti atoms. Its susceptibility indeed has a maximum at ∼2 K and is characterized by $\chi(T \to 0) \to 0$ for $x \leqslant 0.1$. This feature is destroyed with substitution, and the magnetic state is approached; for $x > 0.1$, $\chi(T > T_C)$ follows the Curie–Weiss law. For the series $Fe_2V_{1-x}Ti_xAl$, the magnetic susceptibility data, which allowed us experimentally to obtain the nonmagnetic/magnetic ground state versus x, correlate with the results of band structure calculations. We can draw a schematic phase diagram for $Fe_2V_{1-x}Ti_xAl$ on the T–x plane (or T–n, where n is the changing number of the conduction electrons), which seems to be similar to the diagram proposed for $CeRhSb_{1-x}Sn_x$ system [51]. In the phase diagram for $Fe_2V_{1-x}Ti_xAl$ system, the $x = 0$ member (Fe_2VAl) is nonmagnetic, whereas on increasing x (decreasing n) the members with $x > 0.1$ are magnetic. The magnetic correlations/ordering destroy the gap in the $Fe_2V_{1-x}Ti_xAl$ system. An interesting behaviour in the diagram is observed for Fe_2TiAl, which is metallic with weak magnetism, and its band structure is similar to that of magnetic half-metals (this is, however, not a perfect half-metallic magnetic ground state[4]; in table 1 all LMTO, FPLO and LAPW calculations give a small DOS of ∼0.15–0.25 eV^{-1} at ϵ_F for the majority-spin band, which leads to a non-integer total spin moment).

The large reduction of χ with application of a relatively small dc field could also indicate a Kondo insulating gap, which is usually strongly reduced in the applied magnetic field [54]; another explanation is addressed to the spin-glass-type behaviour [13]. One also could consider both effects.

In the image of the Kondo gap formation the activated behaviour of the conductivity for $x < 0.1$ can be explained by the nonzero carrier concentration n present at the Fermi level and thermal excitation of the conduction electrons across the gap Δ. The gap could be easily

[4] The half-metallic magnetic (ferromagnetic, HMF) materials have the Fermi level inside the energy gap of the partial density of states for one of the spin projections. The concept of a half-metallic ferromagnet was introduced by de Groot *et al*, based on their electronic structure calculations for the Heusler alloys NiMnSb [52] and PtMnSb [53]. The HMFs give rise to 100% spin polarization at the Fermi energy, ϵ_F, which makes them suitable materials for spin-dependent devices and spin injection. The HMF behaviour, however, is dependent on the atomic disorder, which can either lead to appearance of the HMF ground state or destroy it.

disturbed by disorder. Generally the disordering induces the magnetic moment on the antisite Fe defects, that strongly reduces the gap. Likewise, the magnetic susceptibility $\chi \sim n$, as the carriers are activated through the gap, which means that in the low-temperature region χ increases with increasing T. For the thermally activated quasi-particles $\rho \sim 1/n$, since $\chi \sim n$, so that $\rho\chi = \text{const}$, if only the carrier lifetime τ and the effective mass $m^\star$ do not change with either temperature or x, and do not depend on an atomic disorder. This behaviour is characteristic of the $CeRhSb_{1-x}Sn_x$ series and roughly for $Fe_2V_{1-x}Ti_xAl$ below the percolation limit, i.e., for $x < \sim 0.12$–0.15 in spite of the completely different symmetry of the both systems. Supposely, the band gap in Fe_2VAl could be characteristic of a Kondo insulator. The atomic disorder, however, complicates the interpretation of the nature of this gap.

The large resistivity $\rho(T)$-value of the Fe_2VAl and $Fe_2V_{0.9}Ti_{0.1}Al$ alloys between $2\ \text{K} < T < 300\ \text{K}$ could also be explained by this reasoning. It is, however, difficult to understand why the remaining members of the $Fe_2V_{1-x}Ti_xAl$ series, which are also disordered, do not show any negative TCR effect, $d\rho/dT < 0$.

5. Summary

The electronic structure calculations have shown that Fe_2VAl is semimetallic and nonmagnetic, whereas Fe_2TiAl has a magnetic ground state and a pseudogap at the Fermi level with low DOS for one spin direction band. The solid solution $Fe_2V_{1-x}Ti_x$ Al clearly exhibits the effect of the decreasing number of conduction electrons on the gap formation in Fe_2VAl, as well as the change of the magnetic properties across the series. The samples with $x > 0.1$ are magnetic, with an effective moment of $\sim 3.6\ \mu_B$, while the calculations give an magnetic moment of about $1\ \mu_B$. This discrepancy can be explained on the basis of the itinerant character of d-type electrons on Fe atoms. The concentration $x \cong 0.1$ is critical; it separates the nonmagnetic compounds with a hybridization gap from the other magnetic metals.

Acknowledgments

The authors thank the State Committee for Scientific Research (KBN) for financial support from Project No 1 P03B 052 28. Two of the authors (AŚ and JG) acknowledge Grant No 1 PO3B 094 30 from the Ministery of Education and Science.

References

[1] Riseborough P S 2000 *Adv. Phys.* **49** 257
[2] Lee P A, Rice T M, Serene J W, Sham L J and Wilkins J W 1986 *Comments Condens. Matter Phys.* **12** 99
[3] Nishino Y, Kato M, Asano S, Soda K, Hayasaki M and Mizutani U 1997 *Phys. Rev. Lett.* **79** 1909
[4] Schlesinger Z, Fisk Z, Zhang H T, Maple M B, DiTusa J F and Aeppli G 1993 *Phys. Rev. Lett.* **71** 1748
[5] Lue C S, Ross J H Jr, Chang C F and Yang H D 1999 *Phys. Rev.* B **60** R13941
[6] Feng Ye, Rhee J Y, Wiener T A, Lynch D W, Hubbard B E, Sievers A J, Schlagel D L, Lograsso T A and Miller L L 2001 *Phys. Rev.* B **63** 165109
[7] Singh D J and Mazin I I 1998 *Phys. Rev.* B **57** 14352
[8] Weht R and Pickett W E 1998 *Phys. Rev.* B **58** 6855
[9] Weinert M and Watson R E 1998 *Phys. Rev.* B **58** 9732
[10] Guo G Y, Button G A and Nishino Y 1998 *J. Phys.: Condens. Matter* **10** L119
[11] Okamura H, Kawahara J, Nanba T, Kimura S, Soda K, Mizutani U, Nishino Y, Kato M, Shimoyama I, Miura H, Fukai K, Nakagawa K and Kinoshita T 2000 *Phys. Rev. Lett.* **84** 3674
[12] Endo K, Matsuda H, Ooiwa K, Iijima M, Goto T, Sato K and Umehara I 1998 *J. Magn. Magn. Mater.* **177–181** 1437

[13] Lue C S, Ross J H Jr, Rathnayaka K D D, Naugle D G, Wu S Y and Li W-H 2001 *J. Phys.: Condens. Matter* **13** 1585
[14] Deniszczyk J and Borgieł W 2003 *Acta Phys. Pol.* B **34** 1257
[15] Bushow K H J and van Engen P G 1981 *J. Magn. Magn. Mater.* **25** 90
[16] Suzuki R O and Kyono T 2004 *J. Alloys Compounds* **377** 38
[17] Watson R E and Weinert M 1998 *Phys. Rev.* **58** 5981
[18] Palm M, Inden G and Thomas N 1995 *J. Phase Equilib.* **16** 209
Gorzel A, Palm M and Sauthoff G 1999 *Z. Metallkd.* **90** 64
[19] Baer Y, Busch G and Cohn P 1975 *Rev. Sci. Instrum.* **46** 466
[20] Andersen O K 1975 *Phys. Rev.* B **12** 3060
[21] Andersen O K and Jepsen O 1977 *Physica* B and C **91** 317
[22] Singh D J 1994 *Planewaves, Pseudopotentials and the LAPW-Method* (Boston: Kluwer–Academic)
[23] Koepernik K and Eschrig H 1999 *Phys. Rev.* B **59** 1743
[24] von Barth U and Hedin L 1972 *J. Phys. C: Solid State Phys.* **5** 1629
[25] Hu C D and Langreth D C 1985 *Phys. Scr.* **32** 391
[26] Deniszczyk J and Frackowiak J E 1997 *Acta Phys. Pol.* **91** 455
[27] Skriver H L 1984 *The LMTO Method. Muffin-Tin and Electronic Structure* (Berlin: Springer)
[28] Lambrecht W R R and Andersen O K 1986 *Phys. Rev.* B **34** 2439
Kobayashi S and Fujiwara T 1997 *Phys. Rev.* **55** 7445
[29] Andersen O K and Jepsen O 1984 *Phys. Rev. Lett.* **53** 2571
Andersen O K, Jepsen O and Sob M 1987 *Electronic Structure and its Applications* ed M Yussouff (Berlin: Springer) p 2
[30] Perdew J P, Burke K and Ernzerhof M 1996 *Phys. Rev. Lett.* **77** 3865
[31] Singh D J 1991 *Phys. Rev.* B **44** 7451
[32] Blaha P, Schwarz K, Madsen G K H, Kvasnicka D and Luitz J 2001 *WIEN2k, An Augmented Plane Wave + Local Orbitals Program for Calculating Crystal Properties* (Karlheinz Schwarz, Techn. Universitt Wien, Austria) ISBN 3-9501031-1-2
[33] Perdew J P and Wang Y 1996 *Phys. Rev.* B **45** 13244
[34] Koepernik K, Velick B, Hayn R and Eschrig H 1998 *Phys. Rev.* B **58** 6944
[35] Blackman J A, Esterling D M and Berk N F 1971 *Phys. Rev.* B **4** 2412
[36] Eschrig H, Richter M and Opahle I 2004 Relativistic solid state calculations *Relativistic Electronic Structure Theory, Part 2. Applications* (*Theoretical and Computational Chemistry* vol 13) ed P Schwerdtfeger (Amsterdam: Elsevier) pp 723–76
[37] Yeh J J and Lindau I 1985 *At. Data Nucl. Data Tables* **32** 1
[38] Deniszczyk J 2001 *Acta Phys. Pol.* B **32** 529
[39] Soda K, Mizutani T, Yoshimoto O, Yagi S, Mizutani U, Sumi H, Nishino Y, Yokoya T, Shin S, Sekiyama A and Suga S 2002 *J. Synchrotron Radiat.* **9** 233
[40] Tougaard S and Sigmund P 1982 *Phys. Rev.* B **25** 4452
[41] Mooij J H 1973 *Phys. Status Solidi* a **17** 521
[42] Verbeek B H, Nieuwenhuys G J, Stocker H and Mydosh J A 1978 *Phys. Rev. Lett.* **40** 586
[43] Palstra T T, Nieuwenhuys G J, Mydosh J A and Bushow K H J 1985 *Phys. Rev.* B **31** 4622
[44] Wertheim G K, Wernick J H and Sherwood R C 1969 *Solid State Commun.* **7** 1399
[45] Chien C L and Liou S H 1985 *Phys. Rev.* B **31** 8238
[46] Ślebarski A and Spałek J 2005 *Phys. Rev. Lett.* **95** 046402
Spałek J, Ślebarski A, Goraus J, Spałek L, Tomala K, Zarzycki A and Hackemer A 2005 *Phys. Rev.* B **72** 155112
[47] Doradziński R and Spałek J 1997 *Phys. Rev.* B **56** R14239
[48] Aliev F G, Moshchalkov V V, Zalyalyutdinov M K, Pak G I, Scolozdra R V, Alekseev P A, Lazukov V N and Sadikov I P 1990 *Physica* B **163** 358
[49] Takabatake T, Nakazawa Y, Ishikawa M, Sakakibara T, Koga K and Oguro I 1988 *J. Magn. Magn. Mater.* **76/77** 87
[50] Schlottmann P 1996 *Phys. Rev.* B **54** 12324
[51] Ślebarski A, Spałek J, Gamza M and Hackemer A 2006 *Phys. Rev.* B **73** 205115
[52] de Groot R A, Mueller F M, van Engen P G and Bushow K H J 1983 *Phys. Rev. Lett.* **50** 2024
[53] de Groot R A, Mueller F M, van Engen P G and Bushow K H J 1984 *J. Appl. Phys.* **55** 2151
de Groot R A and Bushow K H J 1986 *J. Magn. Magn. Mater.* **54–57** 1377
[54] Aeppli G and Fisk Z 1992 *Comments Condens. Matter Phys.* **16** 155